LANGMUIR

pubs.acs.org/Langmuir Article

ω-Thiolation of Phenolic Surfactants Enables Controlled Conversion between Extended, Bolaform, and Multilayer Conformations

Renaud Miclette Lamarche and Christine DeWolf*

Cite This: *Langmuir* 2020, 36, 2847−2857 Read Online

ACCESS | Metrics & More | Article Recommendations | Supporting Information

ABSTRACT: The self-assembly of ω-thiolated surfactants onto gold is a well-studied phenomenon; however, control over the final organization within the thin films is either limited or requires extensive pre- and post-deposition chemical modifications. On the other hand, Langmuir−Blodgett deposition from the air−water interfaces affords a high degree of control over lateral organization within the film, yet it is generally employed to create physisorbed, soft matter films. Despite this, relatively little is known about the impact of the ω-thiolation on either the air−water of deposited film organization. Here, we show that the introduction of a terminal hydrophilic thiol on a phenolic surfactant does not necessarily disrupt a highly organized film nor does it necessarily induce a bolaform conformation at the interface. We show that the relative proportions of different conformations can be controlled using pH, relaxation time, surface pressure, and combinations thereof. Moreover, at high pH, the system undergoes a monolayer-to-multilayer transition wherein well-defined multilayer structures and morphologies are generated. These multilayers appear to comprise a single bolaform conformation atop an extended-chain condensed phase. We demonstrate that these structures can be transferred using Langmuir−Blodgett deposition demonstrating that combining these two approaches has the potential to achieve greater control over the functional properties of robust, chemisorbed films.

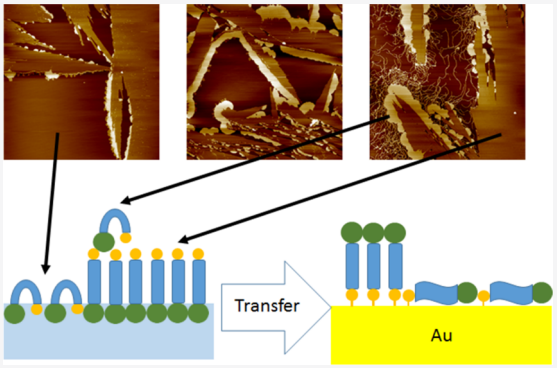

INTRODUCTION

Phenols are the dominant functional moiety of the class of natural compounds called tannins, which can bind histidine-[1] and proline-rich proteins and chelate metals.[2] Combining the phenol functionality into a building block for thin-film self-assembly provides a route to conferring this functionality to a solid surface for biosensing,[3] antifouling,[4] metal binding,[5,6] membrane binding,[7] and oil repellant[8] applications. However, for biosensing applications, which involve binding of a protein, this binding requires insertion of the histidine or proline residue[9] between the phenol moieties; hence, the strength and specificity of such binding is dependent on the distance between the phenols, which must therefore be carefully controlled. Thus, while self-assembled monolayers using thiol-functionalized molecules that chemisorb to gold surfaces[10] provides a facile fabrication route and highly reproducible films, generating a homogeneous surface coverage with a high degree of control over lateral spacing is challenging. One approach is to simply change the terminal functional group of a thiolate-bearing surfactant to a larger functional group, which then defines the lateral spacing[11] and which can later be functionalized. However, this does not necessarily provide the means to generate a homogeneously spaced, low-density film required for an analyte such as proteins to bind. Such a film can be achieved by self-assembling a surfactant with a removable spacer[12,13] wherein this moiety controls the lateral spacing upon chemisorption and can be subsequently cleaved in mild conditions leaving behind a smaller functional group. However, generating the terminal phenol then requires an additional step of chemical modification. In this work, we investigate the possibility of preorganizing thiol-terminated phenol surfactants at the air−water interface and their subsequent Langmuir-Blodgett deposition as a means to control the lateral spacing in the film.[14]

Surfactants can be spread at the air−water interface at molecular areas that correspond to monomolecular films.[15] The film is then compressed to alter the organization and lateral spacing between the surfactants. These methods introduce multiple variables that can influence the lateral spacing within the film, including surface pressure,[16] subphase pH,[17] temperature,[18] and subphase composition.[19] Our previous work showed that the lateral organization, on both the microscopic (domain morphology) and nanoscopic (surfactant organization within domains), can be modified in

Received: November 27, 2019
Revised: February 26, 2020
Published: February 26, 2020

https://dx.doi.org/10.1021/acs.langmuir.9b03670
Langmuir 2020, 36, 2847−2857

films comprising non-ω-thiolated phenolic surfactants by varying the subphase pH wherein the headgroup protonation state alters the intermolecular interactions.[20]

Despite the wealth of literature on both self-assembly of thiolated surfactants on gold and Langmuir–Blodgett (LB) depositions of non-thiolated surfactants (reviewed, for example, by Matharu et al.[21]), there are relatively few studies reporting the Langmuir monolayer behavior of ω-functionalized surfactants.[14,22,23] The possibility of preorganization of surface-active building blocks at the air–water interface and their subsequent deposition opens avenues for an improved degree of control over lateral film organization and structure. Herein, we investigate the impact of adding an ω-thiolation of octadecylgallate to form 18-mercaptooctadecyl 3,4,5-trihydroxy benzoate (ODG SH, Figure 1) on its Langmuir monolayer behavior and its subsequent deposition onto gold substrates.

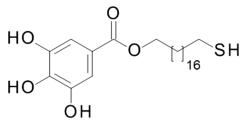

Figure 1. 18-mercaptooctadecyl 3,4,5-trihydroxy benzoate (ω-thiolated octadecylgallate or ODG SH).

MATERIALS AND METHODS

Materials. 18-mercaptooctadecyl 3,4,5-trihydroxy benzoate (ODG SH) was synthesized as reported in the Supporting Information. Ultrapure water (resistivity of 18.2 MΩ/cm) was obtained from an EasyPure II LF system (Barnstead, Dubuque IA). The spreading solutions were prepared using chloroform (HPLC grade, trace of ethanol as preservative) from Fisher Scientific Company. Mica (grade V1) used in the AFM deposition was purchased from Ted Pella, Inc. and freshly cleaved before each measurement. Gold substrates were purchased from Evaporated Metal Films (Ithaca, New York; product # TA134) with a thickness of 100 nm, with a titanium binding layer of 5 nm. These were cut into slices of approximately 1 cm by 2.5 cm. Prior to deposition, these were cleaned using a UVO-cleaner model 342 (Irvine, California) for 15 min. The slides used for air–water deposition were then left in ethanol for 1 h to be chemically reduced[24] and become hydrophobic (contact angle of 99 ± 3°). Slides were reused by removing the monolayer using 0.5 M $NaBH_4$ (Fisher Chemical) in 1:1 ethanol/water[25] and cleaned by ozone for 1 h. Template-stripped gold was made by depositing 100 nm of gold onto a silicon wafer and glued to a glass slide using UV-activated glue (Norland Optical Adhesive). The slides were treated the same as the purchased slides for air–water deposition purposes (15 min ozone clean, 1 h in ethanol) but were not reused.

Isotherm Measurements. Monolayers were spread from a chloroform-spreading solution (1 to 1.5 mM) on two different types of subphases: ultrapure water (pH = 5.5 at 25 °C) and ultrapure water that was adjusted to higher pH using NaOH. Surface pressure–area isotherms were obtained on Langmuir film balances (Nima Technology, Ltd., Conventry, U.K.) at room temperature with a compression speed of 5 cm^2/min (equivalent to between 3 to 7 $Å^2$ $molecule^{-1}$ min^{-1} depending on spreading solution concentration). Two different Langmuir film balances were used, one with dimensions of 5 cm by 35 cm and one with dimensions of 7 by 15 cm for Brewster angle microscopy and ellipsometry measurements. Surface pressure measurements were made using a filter paper Wilhelmy plate (Whatman no. 1 paper). Monolayers were given 10 min for film relaxation prior to compression, unless stated otherwise. Monolayers were transferred at a constant surface pressure onto mica (physisorbed) or gold (chemisorbed) on the upstroke using the Langmuir–Blodgett (LB) technique with a dipping speed of 1 mm/min. Hydrophilic mica was used for traditional LB upstroke transfers where the atomically flat nature of mica enables high-resolution imaging of the phases present. All transfer ratios were always close to 1 for the mica deposition. Hydrophobic gold was also used on the upstroke wherein the convex meniscus allows contact with the exposed thiols. The significantly greater roughness of the gold limits the resolution of the different phases; thus, this was used primarily to evaluate transfer and subsequent chemisorption.

Brewster Angle Microscopy (BAM). Brewster angle microscopy was carried out with an I-Elli2000 imaging ellipsometer (Nanofilm Technologies GmbH, Göttingen, Germany) equipped with a 50 mW Nd:YAG laser (λ = 532 nm). All experiments were performed using a 20× magnification with a lateral resolution of 1 μm. BAM experiments were performed at an incident angle of 53.15° (Brewster angle of water) and a laser output of 50% (analyzer, compensator, and polarizer were all set to 0).

Ellipsometric measurements at the air–water interface were carried out at an incident angle of 50.00° and a laser output of 100%, with the compensator set to 20.00°. The reported measurements are an average of 10 measurements each taken at a different location on the same film and is consistent for multiple samples. The ellipsometric isotherm is reported in terms of $\delta\Delta$, which is defined as the difference between the ellipsometric angle Δ of the film on the subphase and the subphase alone ($\delta\Delta = \Delta_{film} - \Delta_{subphase}$). The reference, 0, is the pure subphase before the film is spread. The measurements were taken at constant surface pressure. $\delta\Delta$ is directly proportional to the thickness of the films when the angle Ψ is constant (for monolayers at the air–water interface, the variations in Ψ are very small). Modeling only one angle does yield reliable thickness values, and hence, $\delta\Delta$, which is independent of an optical model, is reported.

Ellipsometric measurements of films deposited onto gold were carried out at an angle of 65.00° and a laser output of 1%, with the compensator set to 45.00°. The optical properties (n and k) of each gold substrate were determined prior to deposition. The refractive index of the monolayer was set at 1.45.[10] Each set of deposition conditions was performed in triplicate, with 5 measurements per deposition at different locations. Film thickness was measured before and after washing with 2 mL of ethanol to remove any unreacted, non-chemisorbed material.

Atomic Force Microscopy (AFM). A Nanoscope IIIa (Digital Instruments, Santa Barbara, CA) was used to capture AFM images in air at room temperature using tapping mode at a scan rate of 1 Hz using an etched silicon cantilever frequency of ∼300 kHz, a nominal spring constant of 20–80 N/m, and a tip radius of <10 nm. An oscillation amplitude of 175 mV and medium damping (∼25%) were employed for these measurements. All AFM images are for films deposited onto mica unless otherwise indicated.

Grazing Incidence X-ray Diffraction (GIXD). The GIXD experiments were performed at beamline 15-ID-C ChemMatCARS at the Advanced Photon Source (APS) in Argonne National Laboratory with the following parameters: an X-ray beam wavelength of 1.239 Å, incidence angle of 0.09061, horizontal size of 20 mm, and vertical size of 120 mm, leading to a beam footprint of 20 mm by 7.6 cm. The detector used was the two-dimensional Swiss Light source PILATUS 100K set to single-photon counting mode. Two sets of slits, one placed in front of the detector and the other placed 280.0 mm from the sample, were used to minimize intense low-angle scattering. Experiments were performed at the air–water interface of a 340 cm^2 Langmuir trough where the monolayer was spread and then compressed at rates of 2 and 5 cm^2/min (equivalent to 0.5 and 1.3 $Å^2$ $molecule^{-1}$ min^{-1}, respectively) using a mobile barrier. The measured GIXD data was plotted as contour plots of the intensity as a function of both the horizontal (Q_{xy}) and the vertical (Q_z) scattering vector components. The lattice spacing d_{hk} was obtained from the in-plane diffraction data as $d_{hk} = 2\pi/q_{xy}^{hk}$ where the Miller indices h and k were used to index the Bragg peaks needed to calculate the unit cell parameters for the in-plane lattice.[26,27] Raw data was extracted and patched using software developed by Wei Bu, beamline scientist at ChemMatCARS. The Bragg rods and peaks were fitted with Gaussian

https://dx.doi.org/10.1021/acs.langmuir.9b03670
Langmuir 2020, 36, 2847–2857

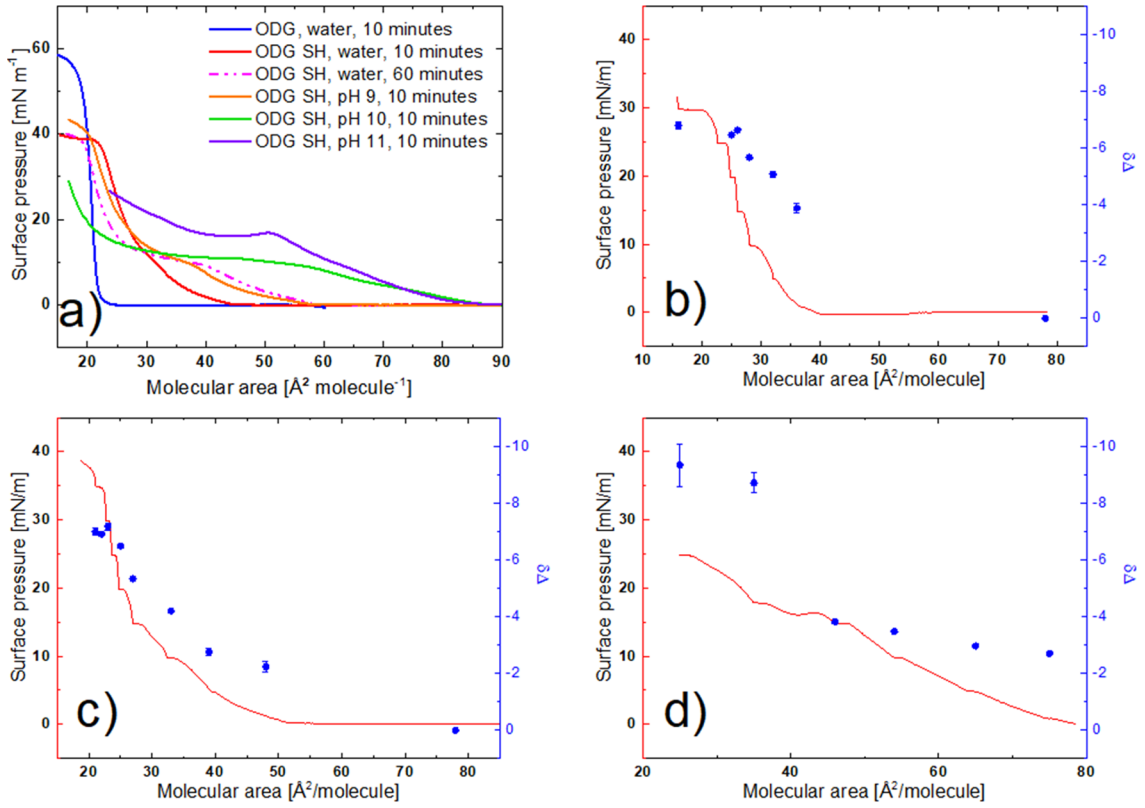

Figure 2. (a) Isotherm of ODG SH on various subphase conditions with different relaxation times (indicated). Ellipsometric measurements at the air−water interface (blue points) along with isotherms in red for (b) ODG SH on water, 10 min relaxation time, (c) ODG SH on water, 60 min, and (d) ODG SH on pH 11 subphase with 10 min relaxation time.

and Lorentzian functions, respectively, using Origin lab graphing and analysis software.

RESULTS AND DISCUSSION

Langmuir Film Behavior. Isotherms for ODG SH under various pH conditions are shown in Figure 2a. On an ultrapure water subphase (pH 5.5, red line), with a standard relaxation time of 10 min prior to compression, ODG SH exhibits a critical area of 45 Å^2/molecule that is significantly larger than the critical area of 26 Å^2/molecule obtained for the non-thiolated (methyl-terminated) octadecylgallate (ODG, blue line). The large increase in molecular area is much greater than what might be expected simply due to the substitution of the methyl with a thiol, which is of a similar size. A possible explanation for the large increase in critical area is that the molecule adopts a bola conformation[28] wherein the chain bends over such that the thiol acts as a secondary headgroup (sometimes referred to as U-shaped). However, this conformation would be expected to have an even larger molecular area. For example, Lahann et al.[13] used computational methods to estimate the areas required to generate a bent conformation of mercaptohexadecanoic acid self-assembled monolayers. They found that 0.65 nm^2 generated an optimal balance between the area requirements for bending and maximizing hydrophobic interactions between the chains. Given that the critical area lies between the proposed areas for bent chains of similar lengths and the extended chain of ODG, this may indicate the coexistence of both the bola and extended conformations. However, phase coexistence should not be thermodynamically favorable over a broad range of surface pressures for a single component system. The isotherms appear to converge in an area at high compression states, prior to collapse of the ω-thiolated surfactant, suggesting a compression-induced transformation from a bola to an extended conformation.

To probe the possibility of the coexistence of and transformation between kinetically and thermodynamically favored phases, the monolayer was left to relax for 60 min prior to compression (pink dashed line, Figure 2a). This leads to an even greater critical area of 60 Å^2/molecule, almost triple that of the methyl-terminated surfactant. This would suggest that immediately upon spreading, the molecule initially adopts an extended formation, with the thiol oriented toward air, but that this organization is only metastable, with a conversion to a bent, bola conformation, that is, with both functional groups in contact with the water, occurring over time. Additionally, after the longer relaxation period, the isotherm clearly exhibits a phase transition plateau around surface pressure of ∼10 mN/m. Such a plateau is usually associated with a first-order phase change in the monolayer.[29] Beyond this plateau, the area approaches the molecular areas obtained upon compression 10 min after spreading and the areas of the methyl-terminated surfactant, suggesting that compression of the film forces a return to an extended conformation as these areas are too small for the bola conformation. Upon closer examination of the isotherms with only 10 min relaxation time, a small kink in the isotherm can be discerned at 10 mN/m. The ODG SH monolayers all collapse at a lower surface pressure, around 40 mN/m, compared to the collapse pressure of approximately 55 mN/m for the methylated version, regardless of relaxation time. This is most likely due to the increased solubility brought about by the addition of the ω-hydrophilic thiol group.[30]

https://dx.doi.org/10.1021/acs.langmuir.9b03670
Langmuir 2020, 36, 2847−2857

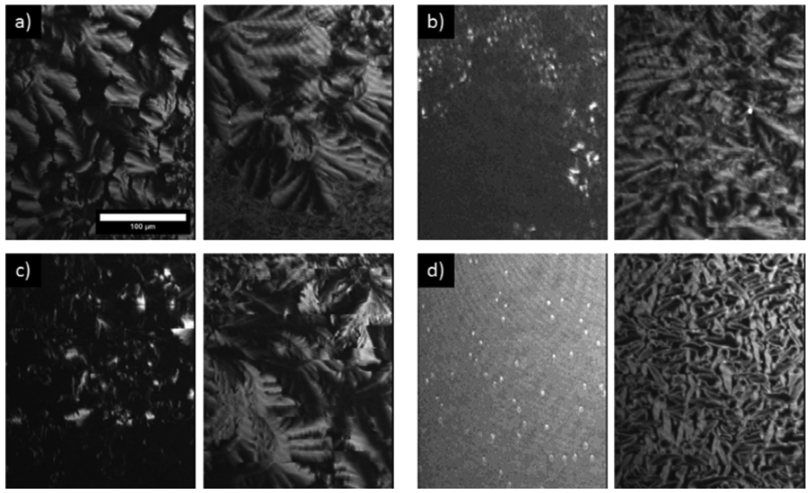

Figure 3. BAM images of ODG SH at below (left) and above (right) the plateau: (a) water, 10 min relaxation time, 5 and 20 mN/m; (b) water, 60 min relaxation time, 5 and 25 mN/m; (c) pH 9, 10 min relaxation time, 1 and 12 mN/m; and (d) pH 10, 10 min relaxation time, 8 and 11 mN/m. Note that the contrast was enhanced for the low surface pressure images of b and d.

BAM imaging was used to further elucidate the nature of the plateau. Representative images of ODG SH on a water subphase with either a 10 or 60 min relaxation time at surface pressures above and below the plateau pressure are shown in Figure 3a,b. For the film with a short relaxation time, large domains with a mosaic texture (Figure 3a) are observed at both low and high surface pressures, attributed to a condensed phase formed by extended chains. Increasing the relaxation time (Figure 3b) leads to a surface bereft of mosaic domains at low surface pressure (5 mN/m). There is evidence of small bright domains, which are not sufficiently large to observe the internal anisotropy, if present. Compressing the film into the plateau leads to the recovery of the mosaic texture. Assuming the mosaic texture to be associated with the extended form, this provides further evidence that an extended-to-bola transformation takes place over time at high molecular areas but the reverse bola-to-extended transformation can be induced with compression via a first-order phase transition. Such a bent-to-extended transition has been reported in the literature for the similar length 1,18-octadecanedicarboxylic acid[31] and longer bola amphiphiles.[28]

Such a phase transition should be evident from monolayer thickness changes over the course of the isotherm, which can be evaluated using ellipsometry. These measurements do not directly measure the thickness of the monolayer but rather measure the change in ellipsometric angles, which can be correlated to relative changes in optical properties including optical thickness.[32] The ellipsometric isotherms are presented in Figure 2b,c and show that the monolayer with minimal relaxation time exhibits a large initial increase in the ellipsometric angle Δ (which is directly correlated to the thickness) once the critical area is reached, after which further compression yields only a modest increase in $\delta\Delta$. It is important to note that the laser footprint is much larger than the domains at the air−water interface; thus, the $\delta\Delta$ represents an average over the surface. A phase coexistence of condensed phase domains dispersed within a thinner matrix (gas or liquid-expanded phase) will lead to a film thickness that is not representative of the domain thickness, especially at low surface pressures, and the modest increase in $\delta\Delta$ may reflect a reduction of the proportion of the gas phase present at the surface instead of or in addition to a film thickness increase.

In order to probe the domain structure with higher-resolution films, AFM imaging of an LB film deposited onto mica at 5 mN/m from a water subphase (Figure 4a) was

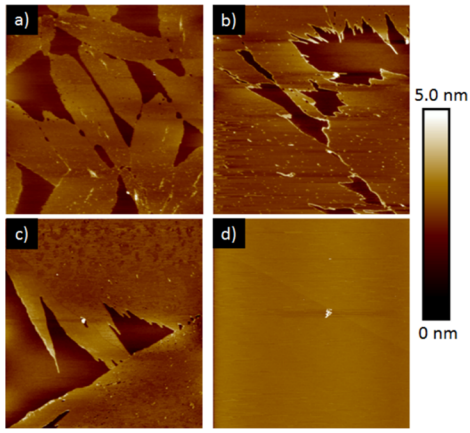

Figure 4. AFM images of ODG SH deposited onto mica at 5 mN/m with variations in subphase, relaxation time, and image size: (a) water, 10 min, 5 μm; (b) water, 60 min, 5 μm; (c) pH 9, 10 min, 5 μm; and (d) pH 9, 60 min, 20 μm.

carried out and confirms a coexistence of condensed phase domains within a matrix, which is 0.94 ± 0.18 nm lower in height. Deposition of this monolayer at higher surface pressure (20 mN/m, Figure S1) shows a uniform surface corresponding to a full coalescence of the condensed phase domains and exclusion of any residual gas or liquid phase. Referring to the ellipsometric isotherm, at 20 mN/m, the thickness of the film no longer increases significantly, supporting the conclusion that the increase in Δ observed results from exclusion of the thinner phase. In contrast, the ellipsometric measurements for the film with the longer, 60 min relaxation time (Figure 2c) show a more modest initial $\delta\Delta$ and a gradual increase in $\delta\Delta$ with compression. At higher surface pressures, similar values of $\delta\Delta$ are reached with both monolayers, indicating that the final thickness achieved is the same regardless of relaxation time, consistent with an extended conformation at high surface pressures. AFM deposition for the latter film at low surface pressures (below the plateau) also shows a coexistence of

https://dx.doi.org/10.1021/acs.langmuir.9b03670
Langmuir 2020, 36, 2847−2857

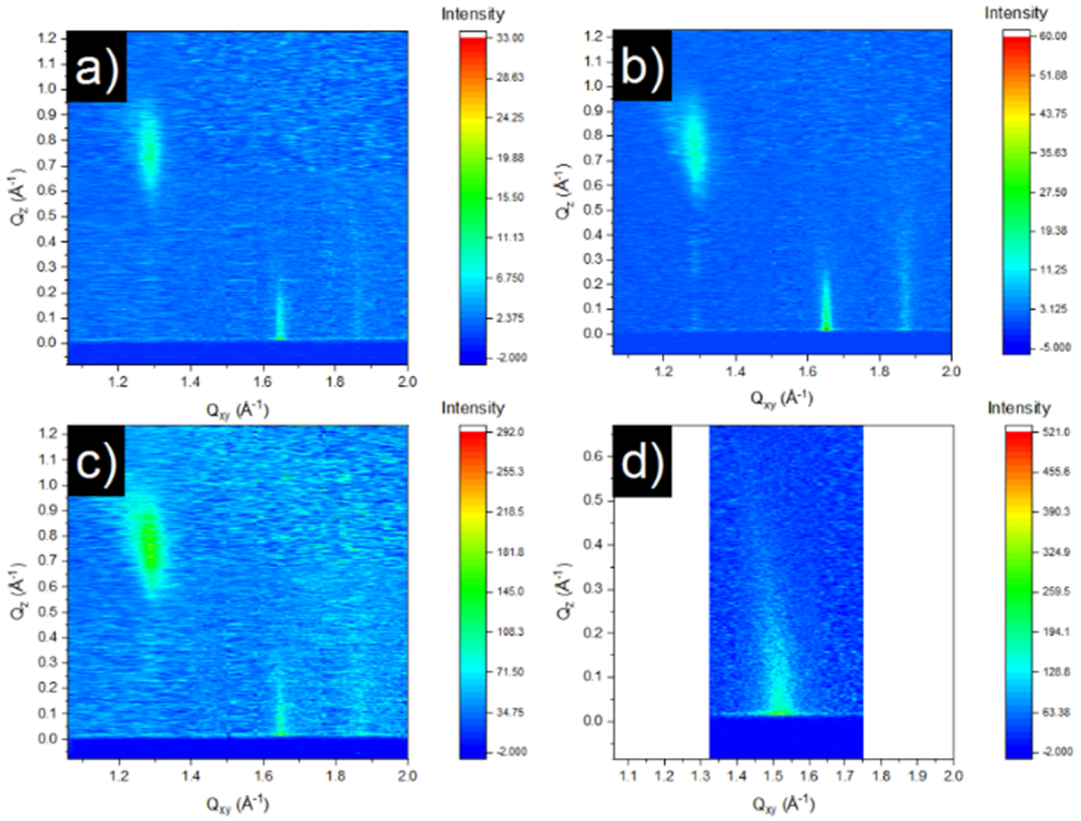

Figure 5. GIXD contour plots of the X-ray diffraction intensity as a function of the in-plane (Q_{xy}) and out-of-plane (Q_z) vector components for ODG SH: (a) water, 1 mN/m; (b) water, 20 mN/m; (c) pH 10, 5 mN/m; and (d) pH 10, 15 mN/m.

condensed phase domains (Figure 4b), but the domain edges are more frayed and less rounded, consistent with the proposal that edge molecules convert to bolaform (the surrounding matrix).

GIXD provides information about the lateral structure of the condensed phase formed. A GIXD contour plot of the diffraction intensity as a function of the in-plane (Q_{xy}) and out-of-plane (Q_z) components of the scattering vector for ODG SH on water is shown in Figure 5a with the corresponding unit cell parameters in Table 1. The peak positions (Table S1) and hence unit cells are identical to those reported previously for the methyl-terminated ODG surfactant, including the peak at Q_{xy} = 1.86 Å^{-1} that we previously attributed to a supermolecular lattice unit cell due to headgroup ordering.[20] It is assumed that in the extended configuration, the phenol is oriented toward the subphase and the thiol is extended toward air. Although a mixed orientation cannot be explicitly excluded, the identical diffraction patterns for methyl- and thiol-terminated surfactants and the lack of broadening of the peaks (i.e., identical correlation lengths) do not support a mixed orientation. The GIXD data not only confirms that the condensed phase observed by BAM and AFM corresponds to the extended conformation; additionally, the presence of the ω-thiol has no impact on the structure of the condensed phase formed by the extended surfactants. This highlights the strength of the non-covalent interactions between the headgroups, which dominates the organization leading to a supermolecular lattice in addition to an alkyl chain lattice wherein even the addition of the ω-thiol does not disrupt this organization.

Table 1. Alkyl Chain Unit Cell Parameters Derived from GIXD for ODG SH at Room Temperature on Various Subphases[a]

pressure (mN/m)	a (Å)	b (Å)	γ (°)	t (°)	Ψ	thickness of the alkyl chain region (nm)
water						
1	7.60	6.35	90	39	NN	2.40
20	7.58	6.37	90	39	NN	2.40
pH 10 subphase						
5	7.58	6.37	90	39	NN	2.40
15	8.31	4.84	90	15	NN	3.0

[a] a, b, γ are the unit cell dimensions based on rectangular nomenclature, t is the tilt angle relative to normal, Ψ is the tilt direction relative to the unit cell where NN represents a tilt towards nearest neighbor, and the approximate thickness of the alkyl chain region was estimated from the tilt angle and length of full extended surfactant.

Impact of pH on Langmuir Film Behavior. The rigid organization imposed by strong headgroup interactions can be disrupted by increasing the subphase pH, attributed to deprotonation of two of the headgroup hydroxyls.[20] Similarly for ODG SH, modifying the subphase pH may alter either or both the molecular conformations or the kinetics of conformational changes. The isotherm of ODG SH on a pH 9 subphase (10^{-5} M NaOH) is shown in Figure 2a. At this pH and with 10 min relaxation time, the isotherm shows similar behavior to that observed on water with the longer relaxation time, namely, the shift to higher molecular areas and the appearance of a plateau in the isotherm at approximately 10 mN/m. BAM images (Figure 3c) confirm the similarity in the morphological

https://dx.doi.org/10.1021/acs.langmuir.9b03670
Langmuir 2020, 36, 2847−2857

features of these two films with small domains below the plateau (as well as some anisotropic regions) and complete coverage of the mosaic texture (anisotropic) film above the plateau. Similarly, AFM shows frayed domains (Figure 4c and Figure S3 of the Supporting Information) as seen for longer relaxation time on a water subphase. We have previously shown that increasing the pH of the subphase with ODG leads to smaller domains, most likely due to interdomain electrostatic repulsion,[20] even when the organization at the molecular level within the domains is unperturbed. For ODG SH, the increase in pH increases the rate of conversion from an extended to a bola conformation. Assuming that this transition is initiated at domain boundaries (likely leading to the frayed domain edges) where the surfactants have sufficient space and conformational freedom to bend over, then the increased rate of conversion correlates with a higher proportion of perimeter molecules that occurs with smaller domains. Combining an increase in pH and a longer relaxation time yields a greater increase in molecular area (Figure S4), demonstrating that the system is not yet at equilibrium. Under these conditions, BAM (Figure S5) and AFM (Figure 4d and Figure S6) images reveal a different morphology: below the plateau, no features are seen, most likely indicating that the system is fully in the bola conformation, which cannot coalesce into discrete domains. With the onset of the plateau, small condensed phase domains attributed to the extended conformation appear. This indicates that although the pH impacts the rate of conversion, the fundamental organization of the system is unchanged and the bent-to-extended transition can still be induced with compression of the film.

These effects are accentuated with increasing pH. At pH 10, shifts to higher molecular areas are observed (Figure 2a green), confirming a greater proportion of molecules with the bent, bola conformation or in other words, a greater rate of conversion between the initial phase of extended conformation and the bent conformation phase formed upon relaxation at the surface. BAM (Figure 3d) and AFM (Figure 6a) imaging show the presence of some well-dispersed, small, condensed phase domains (1.5 to 1.7 nm above the background) below the plateau. This height difference between the two phases is higher than what was obtained at lower pH (for which the height difference was approximately 0.95 nm). It is not known whether the condensed phase domains are thicker or the bolaform matrix is thinner; however, as will be shown below, the GIXD indicates that the tilt angle of the condensed domains present up to the plateau remains the same, indicating that the bola phase must be thinner, which may be due to charge repulsion between deprotonated headgroups. It is thought, based on our previous work, that the gallate begins to undergo a second deprotonation at this pH. However, the thiol must additionally be taken into account for which a pKa of approximately 10.5 has been reported.[33]

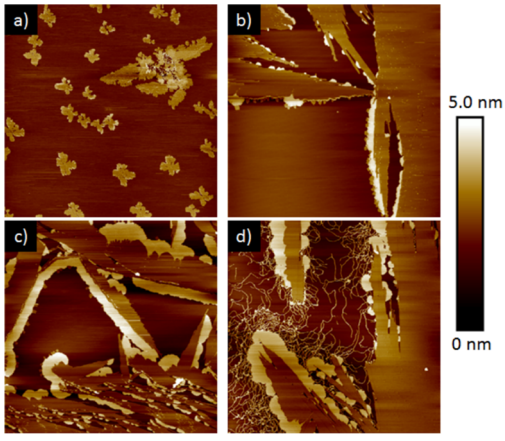

Figure 6. AFM measurement of ODG SH deposited onto mica from a pH 10 subphase at surface pressures of (a) 5 mN/m, 25 μm; (b) 10 mN/m, 25 μm; (c) 14 mN/m, 15 μm; and (d) 16 mN/m, 15 μm.

BAM shows the growth of irregularly shaped domains at the beginning of the plateau (Figure 3d and Figure S7). As the domains grow, the internal anisotropy becomes apparent with the brightness of the domain being a function of its orientation relative to the incoming polarized light. Many of the domains feature a dark interior with a brighter perimeter; notably, these domains are oriented in the same direction (i.e., the long axis of the domain is horizontal with respect to the image, see highlighted domains in Figure S7), while the brighter features are oriented vertically with respect to the image. AFM imaging was used to determine if the bright perimeter material is different from the dark interior or if this is simply a manifestation of the anisotropy. These images reveal a very unusual morphology (Figure 6b–d and Figure S8 of the Supporting Information) with three phases with distinct heights. At the start of the plateau (Figure 6b), we again observe the large, frayed-edge domains that are approximately 1.75 ± 0.14 nm higher than the surrounding matrix in height. Additionally, small bright regions are observed at the domain boundaries, which are 3.12 ± 0.14 nm above the background matrix. Initially, these appear as rounded nodules decorating the domain boundary (Figure 6b). As the surface pressure increases, these nodules coalesce to generate a more continuous band of material outlining the condensed domain. The lateral thickness of the band is reasonably consistent between domains and does not appear to grow beyond 1−2 μm from the domain edge. As the film emerges from the plateau, filaments appear to form extending from the continuous band of higher material. There is a higher density of these filaments near the edges of the band of higher material, but they can extend throughout the background matrix (Figure 6d) and the filaments are the same height as the continuous band, namely, 3.12 nm above the matrix. Notably, in Figure 6d (Figure S8 for a magnified view), the small round domains of the same material appear to nucleate at the junctions of filaments, which may grow to form the larger domains of these materials observed in Figure 6d and Figure S8. Notably, this morphology appears to be extremely sensitive to deposition conditions, that is, the intermediate stages are not always observed and films comprising only the round domains surrounded by a high density of filaments, in the absence of the intermediate height condensed domains, can also be observed.

GIXD measurements were performed below and above the plateau region (1, 5, and 15 mN/m, Figure 5 and Table 1). At the lowest surface pressure, no discernible diffraction pattern was observed, and this was attributed to a low density of any residual extended form, condensed phase material. At 5 mN/m, the organization is identical to that observed for both the thiol- and methyl-terminated surfactants on a water subphase for which the tilt angle was invariant with compression. At the plateau, a transition takes place with a step change to less-tilted structure (tilt angle of 15° from the normal, versus 39° from the normal at lower surface pressure and on water at all surface

https://dx.doi.org/10.1021/acs.langmuir.9b03670
Langmuir 2020, 36, 2847−2857

pressures). Additionally, the high Q_{xy} peak attributed to headgroup ordering is no longer present. If both the frayed domains and the band of higher material surrounding them are assumed to be liquid crystalline, either two diffraction patterns should be observed or one if they have identical organizations. However, if the band of higher material were to be fully organized, one would expect to see bending of the peaks along the Debye−Scherrer line to reflect the three-dimensional nature of the structures.[34,35] Given that neither of these are the case, two assumptions can be made: the plateau corresponds to the transition between the two tilted structures, and concurrently, the higher material is formed and is amorphous.

Using this information, we can attempt to identify the various features seen by AFM. The background matrix is most likely the surfactant in bolaform, which is not in a condensed phase and therefore does not generate a diffraction pattern. Just below the plateau, domains appear, which correspond to the more tilted phase (Figures 7a and 5c). At the phase

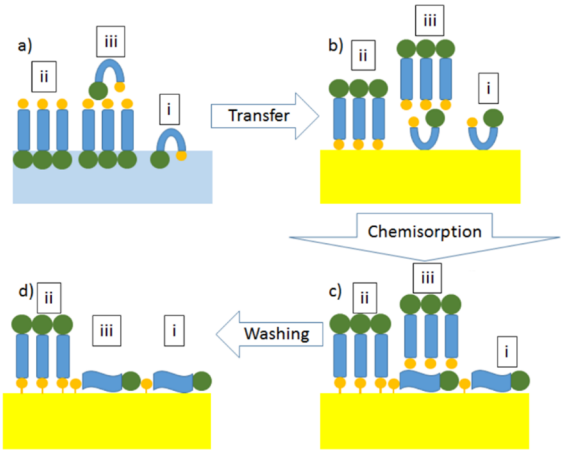

Figure 7. (a) Schematic representation of the various phases formed by ODG SH on a pH 10 subphase at high surface pressure; proposed sequence of events that may take place during (b) transfer, (c) chemisorption, and (d) subsequent washing of films transferred in the high-pressure, multiphase regime. Three different configurations are schematically depicted: (i) bent bolaform, (ii) extended form, and (iii) multilayered composed of a bent conformation atop an extended monolayer.

transition, the frayed-edge domains are generated, which must correspond to the lower tilt angle phase seen by GIXD in agreement with the increased height difference observed with AFM. The film thickness has been estimated from the molecular length (3.1 nm full extended) and the tilt angle in Table 1. For the phase with a 15° tilt angle, the maximum thickness would be 3.0 nm. Given that these domains are only 1.8 nm above the background, it can be assumed that the background matrix comprises the bent bola conformation and precludes that this is simply uncovered mica. The bola phase must therefore have a thickness of approximately 1.2 nm. This is in reasonable agreement with a bent chain conformation, assuming a tight turn, which can be achieved even with only six carbons involved in the turn.[36] The highest phase (3.1 nm above the bola phase) is too high to be a single monolayer. The height difference between the higher material and the domains in which they are in contact with is 1.4 nm (the tallest phase to intermediate phase), which is in reasonable agreement with another bola layer. We therefore propose that the material in this highest phase is not a traditional multilayer but rather a combination of an underlying condensed phase with the molecules in extended form upon which sits an additional layer in bolaform (Figure 7a, iii). This would allow the surfactant to maximize the interactions between polar moieties, the thiol at the end of the condensed phase and both the thiol and phenol of the bola phase, leaving the bola chain exposed. Compressing bola surfactant monolayers often results in multilayer formation,[37−39] but to the best of our knowledge, there are no reports of a multilayer combining the layers of extended molecules with layers of bent conformation molecules. This difference may be derived from the molecular structure: these prior studies[37−39] used symmetrical bola amphiphiles, whereas here, we report on an asymmetric ω-thiolated phenolic bola surfactant.

Although the methyl-[20] and thiol-terminated surfactant condensed phases show identical organizations and tilt angles on water, the impact of headgroup deprotonation leads to very different tilt angles at high pH as well as a difference in the pH required for deprotonation. Assuming the phenolic headgroup retains a similar pK_a, which is not unreasonable given the similarity in phase behavior, this would indicate that once the headgroup organization is disrupted (loss of the high Q_{xy} peak), the ω-thiol has a much more significant impact on the phase behavior. The change in the packing and tilt angle is likely driven by maximizing thiol−thiol non-covalent interactions.

Since the filaments observed using AFM for films deposited from a pH 10 subphase (Figure 6d) are of the same height as the nodules formed (the highest phase), we assume that they correspond to the same phase. This is supported by the observance of only a single diffraction pattern by GIXD. Given that the nodules appear at lower surface pressures (the beginning of the plateau) while the filaments appear only at the end of the plateau, this might suggest that the formation of the multilayer can occur via different routes. They initially form only at the edges of the condensed phase domains indicating that the phase boundary catalyzes and nucleates the formation of the multilayer phase. Once the frayed domain perimeter is mostly covered, a new nucleation mechanism results in the long filaments. Linear nanostriped multilayers formed by bolaamphiphiles were reported by Chen et al.;[38] although in this case, the multilayered bolaamphiphile was proposed to be in an upturned bent conformation, that is, the orientation was driven by hydrophobic interactions. They based their conclusion on a prior report in which traditional, single-headgroup surfactants could form linear multilayers along defect lines.[40] In both of these reports, these defects at which multilayer formation occurred were attributed to the mismatch of the area requirements of the polar groups and the hydrophobic chains. In our case, this mismatch may be amplified by the strong headgroup interactions and non-equivalent headgroups that may be driving molecular alignment.

The methyl-terminated surfactant has a tendency to form a condensed phase with highly directional growth at high pH,[20] which has been attributed to strongly oriented headgroup interactions. Such interactions can also dominate with the bolaform surfactant, for example, a symmetric phenolic bola surfactant by Liu et al.[41] showed strong tendency to form filamentous domains but only when the alkyl chain number was odd, otherwise, 3D nanostructures were formed. This was attributed to the presence of strong directional interactions

https://dx.doi.org/10.1021/acs.langmuir.9b03670
Langmuir 2020, 36, 2847−2857

between both the phenol headgroups and the amide connections to the chains, which then limited the conformation freedom of the alkyl chain. The difference in chain lengths (odd versus even) led to changes in the dipolar interactions between the amides resulting in the different either parallel or antiparallel arrangements (filaments or 3D structures).

Spreading the monolayer on a pH 11 subphase does not cause further increase in the critical area (Figure 2a) but induces a slight increase in the plateau pressure. As was observed on the pH 10 subphase, no features are visible by BAM before the plateau (with the exception of a 2D foam structure directly after spreading, Figure S9 of the Supporting Information). Again visible domain formation begins with the plateau, with a different morphology. Initially, small, bright domains are observed within a non-homogeneous background. At 20 mN/m, these domains appear to coalesce with only a few residual holes visible (Figure S9 of the Supporting Information). AFM images taken of films deposited below the plateau are mostly flat with the occasional small domain that would be at the limit of the resolution of BAM. The domains have a height between 1.5 and 2.5 nm (Figure S10a of the Supporting Information) above the continuous phase and display significant roughness. It may be that these domains are remnants of the extended form of the surfactant, which has not converted into bolaform prior to compression. GIXD of the film at 5 mN/m shows no discernible diffraction peaks, indicating that the continuous phase is likely the bolaform surfactant and that there are not sufficient condensed phase domains present within the beam footprint to generate a diffraction signal. Above the plateau, AFM shows the coexistence of filaments and small round domains that are 2.7 ± 0.2 nm above the continuous bolaform phase, that is, at no stage, only circular domains or filaments are observed (Figure S10b of the Supporting Information). The circular domains are at the limit of the resolution of BAM. At this pH and surface pressures above the plateau, there is no evidence of the intermediate height phase that was observed at pH 10. Despite this, GIXD confirms the presence of the low tilt angle phase (Figure S11), similar to what is seen at pH 10. However, the signal is weak, such that the exact position of the out-of-plane peak cannot be fit with confidence. Evidence that the phase is still tilted (i.e., that there is a second peak, which resides at $Q_z > 0$ Å^{-1}) derives from the peak widths. The in-plane peak is at a very similar position (Q_{xy} of 1.48 Å^{-1} at pH 11 compared to 1.51 Å^{-1} for pH 10), but fitted as a single peak, this would yield an FWHM in Q_z that is far too high for a C18 alkyl chain (see Table S1 for GIXD peak fits). The weak GIXD peaks are most likely due to a smaller-area surface coverage by this phase. Given the lack of evidence of an intermediate height (condensed) phase in the AFM images at these surface pressures, it can only be concluded that this low tilt condensed phase must reside underneath the small domains and filaments. Ellipsometric measurements at the air−water interface show a significant step change in $\delta\Delta$ at the plateau region, which also reaches greater (more negative) $\delta\Delta$ values (Figure 2d).This is consistent with a transition from a predominantly bola phase with very few condensed phase domains to a multilayered phase. Notably, the surface homogeneity in this phase-separated system was low, resulting in large errors on the measurements at high surface pressures. Thus, it appears that increasing the charge on the phenolic headgroup limits the ability to form the condensed phase unless a multilayer can be formed concurrently. This may be due to the additional stabilizing non-covalent interactions between the thiol and the phenol when a multilayer is formed.

LB Deposition onto Gold Substrates. Deposition of the thiol onto gold for chemisorption was achieved via both self-assembly and LB deposition from the air−water interface. The self-assembled monolayers (SAMs) of ODG SH exhibit a postwash thickness of 3.81 ± 0.16 nm as determined by ellipsometry. This is thicker than the length of the fully extended surfactant (3.1 nm), indicating some degree of multilayer formation. Visualization of the surface using imaging ellipsometry did not reveal any features (data not shown); therefore, any form of multilayer must be homogeneously distributed across the sample, at least on the micrometer scale.

Deposition from a water subphase as a function of surface pressure (Figure 8, blue line) shows two deposition regimes,

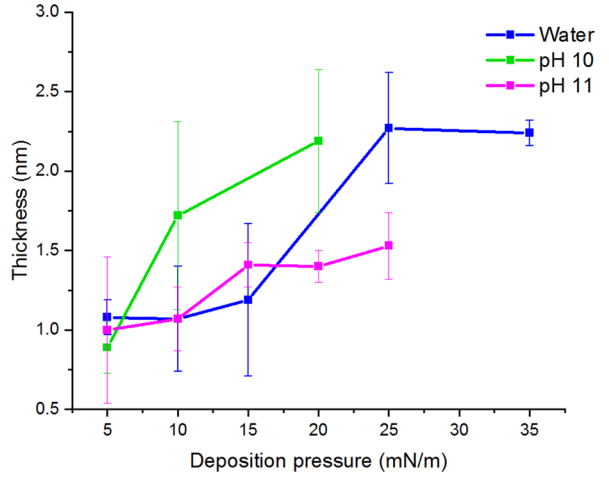

Figure 8. Deposition thickness obtained by ellipsometric measurement of ODG SH transferred onto a gold substrate using LB deposition from the air−water interface as a function of deposition pressure for different pH subphases.

either side of the isotherm kink/plateau, the surface pressure at which the bolaform surfactants are forced upward due to surface pressure. Thus, at 15 mN/m, the larger standard deviation is a consequence of depositing within the plateau region where the films feature a mix of both bola and extended forms. The increase in thickness at surface pressures of 15 mN/m and above must derive from the variation in the proportion of these two forms since it was shown by GIXD that the organization of the condensed phase, and therefore its thickness, is constant during the compression. Thus, the increase must come from the exclusion of any remaining bolaform still present at the air−water interface. Once all of the bolaform is fully converted to extended form, the thickness stabilizes (comparing deposition at 25 mN/m and 35 mN/m).

Deposition of the films onto gold substrates from pH 10 subphase shows an earlier, that is, at lower surface pressure, increase in deposition thickness compared to water (Figure 8). This large increase coincides with the appearance of the thicker (frayed-edge) domains observed on mica (Figure 6d), which GIXD confirmed have a lower tilt angle and therefore are thicker than the condensed phase formed on water (Table 1). However, further compression does not yield a large increase in the thickness of the deposited film (compare 20 mN/m to 10 mN/m). At these higher surface pressures, the film at the

https://dx.doi.org/10.1021/acs.langmuir.9b03670
Langmuir 2020, 36, 2847−2857

air−water interface comprises three phases, postulated to be (i) a fluid phase comprising bolaform, (ii) a condensed phase comprising straight form, and (iii) a multilayer comprising a bola form atop the condensed phase (see Figure 7a). Depending on the surface pressure and phases present, not all of the thiols will contact the hydrophobic gold during the LB deposition process in which the outward facing groups (air-side) make initial contact with the gold. Figure 7 depicts a proposed sequence of events that may take place during the transfer, chemisorption, and subsequent washing of films transferred in the high-pressure, multiphase regime that would account for the experimental observations. For the simple bola phase (phase i, Figure 7), although the chain makes initial contact with the gold, the flexibility afforded in this phase enables subsequent rearrangement such that many of the thiols can chemisorb. For the extended-form condensed phase domains (phase ii, Figure 7), the thiol is exposed air-side and therefore easily chemisorbs. For the multilayered phase (phase iii, Figure 7), again, the bola can reorganize to make contact with the gold; however, much of the extended phase upon which the bola resided is either not transferred or blocked from chemisorbing to the gold surface, allowing it to be washed away (Figure 7c,d).

Deposition of the film from a pH 11 subphase onto gold (Figure 8 pink line) indicates a lower film thickness than that observed at lower pH at all pressures and a lack of a significant step change in thickness at the plateau. At low surface pressures, the film at the air−water interface showed no GIXD peaks and is therefore assumed to have only one dominant phase, a fluid bolaform phase, present, which explains the similarity in thickness between all of the films deposited at 5 mN/m. Upon compression, only the multilayered phase and the bola phase are observed (phases i and iii in Figure 7). As described earlier, phase iii does not deposit well, and in the absence of an extended-form condensed phase, only the bola phase deposits to any great extent (i.e., the overlying phase is easily washed away). This results in a small, continuous change in thickness for the deposited films at pH 11, attributed simply to compression of the bent bolaform chains. Even upon higher compression, the thickness never reaches that expected for a condensed phase.

CONCLUSIONS

The formation of highly organized chemisorbed monolayers of long-chain thiols from solution self-assembly is now well established, yet there are relatively few examples of deposition of long-chain thiols from an air−water interface as means to control lateral spacing and film organization.[14] Ihalainen and Peltonen[23] demonstrated that ω-methyldisulfide-terminated phospholipids, in which one of the two alkyl chains terminates with a disulfide moiety, can be deposited with the disulphide exposed for subsequent metal deposition; however, this was for a disulfide rather than a thiol. In this work, we demonstrate that for single chain, condensed phase forming surfactants, the addition of an ω-thiol does not impact the structure of the condensed phase on water. It does, however, impact the overall phase behavior wherein the ω-thiol acts as a second headgroup. Initially, a condensed phase forms, which comprises an identical organization to the methyl-terminated surfactant, that is, the extended conformation of the surfactant. This is, however, kinetically unstable: relaxation over an extended period of time prior to compression allows a significant proportion to convert to a bola conformation wherein both the phenol and thiol are tethered to the water. This is reversible with film compression where the reduction in available surface area will force the surfactants back to an extended conformation, yielding a first-order phase transition (plateau). The kinetics of the transition from extended to bola can be increased by increasing the subphase pH to 9. This is most likely due to the increased electrostatic repulsion between the deprotonated phenols for which the bolaform organization, where the phenols are further apart, is more favorable. Understanding the behavior of such molecules is essential to be able to use the LB deposition as a means to afford control over film organization at the air−solid interface.

Most reports of bola amphiphiles at the air−water interface involve symmetrical molecules. Herein, we report on an asymmetrical molecule such that one headgroup provides the means to tether to the solid surface and will confer functionality to the deposited film. At high pH (pH 10 and above), this results in the coexistence of multiple phases including a multilayer phase. Importantly, unlike systems in which the "collapse" of the film generates an amorphous material and/or irregular multilayers, this asymmetrical bola amphiphile forms a regular, well-defined structure, which is proposed to be a second bola conformation atop the extended-form condensed phase. The evolution of this multilayer, in the forms of nodules decorating the edges of the condensed phase, circular domains, and filaments within a bola matrix, was followed using AFM and GIXD.

Finally, we demonstrated that the monolayer films could be deposited by Langmuir−Blodgett from the air−water interface, generating robust, chemisorbed films. The deposited film thickness, and hence organization, is dependent on the deposition conditions, that is, both the surface pressure and subphase pH, and as such, these can be employed to tailor the lateral spacing between the surfactants. This opens the avenues for a new deposition approach by preassembling ω-thiolated surfactants at the air−water interface.

ASSOCIATED CONTENT

Supporting Information

The Supporting Information is available free of charge at https://pubs.acs.org/doi/10.1021/acs.langmuir.9b03670.

Additional isotherm, AFM and BAM pictures along with GIXD fitted data and deposition thickness information, and synthesis conditions (PDF)

AUTHOR INFORMATION

Corresponding Author

Christine DeWolf − *Department of Chemistry and Biochemistry and Centre for NanoScience Research, Concordia University, Montreal, Quebec H4B 1R6, Canada;* orcid.org/0000-0002-5185-7237; Email: Christine.dewolf@concordia.ca

Author

Renaud Miclette Lamarche − *Department of Chemistry and Biochemistry and Centre for NanoScience Research, Concordia University, Montreal, Quebec H4B 1R6, Canada*

Complete contact information is available at: https://pubs.acs.org/10.1021/acs.langmuir.9b03670

Author Contributions

The manuscript was written through contributions of all authors.

https://dx.doi.org/10.1021/acs.langmuir.9b03670
Langmuir 2020, 36, 2847−2857

Notes

The authors declare no competing financial interest.

■ ACKNOWLEDGMENTS

C.D. acknowledges funding from the Natural Sciences and Engineering Research Council (NSERC) of Canada and the Canada Foundation for Innovation (CFI). C.D. is a member of the multi-institutional Québec Center for Advanced Materials (QCAM). We thank Rolf Schmidt for data discussion. The synthesis was carried out by Violeta Toader whose position is funded by the FRQNT through its financial support to QCAM . The template-stripped gold was prepared by Eric Dionne in Prof. Antonella Badia's laboratory at the Université de Montréal. GIXD was carried out at NSF's ChemMatCARS Sector 15, which is principally supported by the Divisions of Chemistry (CHE) and Materials Research (DMR), National Science Foundation, under grant number NSF/CHE-1834750. Use of the Advanced Photon Source, an Office of Science User Facility operated for the U.S. Department of Energy (DOE) Office of Science by Argonne National Laboratory, was supported by the U.S. DOE under contract no. DE-AC02-06CH11357.

■ REFERENCES

(1) Yan, Q.; Bennick, A. Identification of Histatins as Tannin-Binding Proteins in Human Saliva. *Biochem. J.* **1995**, *311*, 341−347.
(2) Quideau, S.; Deffieux, D.; Douat-Casassus, C.; Pouységu, L. Plant Polyphenols: Chemical Properties, Biological Activities, and Synthesis. *Angew. Chem., Int. Ed.* **2011**, *50*, 586−621.
(3) Çakıroğlu, B.; Özacar, M. Tannic Acid Modified Electrochemical Biosensor for Glucose Sensing Based on Direct Electrochemistry. *Electroanalysis* **2017**, *29*, 2719−2726.
(4) Xu, L. Q.; Pranantyo, D.; Ng, Y. X.; Teo, S. L.-M.; Neoh, K.-G.; Kang, E.-T.; Fu, G. D. Antifouling Coatings of Catecholamine Copolymers on Stainless Steel. *Ind. Eng. Chem. Res.* **2015**, *54*, 5959−5967.
(5) McDonald, M.; Mila, I.; Scalbert, A. Precipitation of Metal Ions by Plant Polyphenols: Optimal Conditions and Origin of Precipitation. *J. Agric. Food Chem.* **1996**, *44*, 599−606.
(6) Khedimallah, N.; Zazoua, A.; Sbartai, A.; Jaffrezic-Renault, N. A High Sensitivity Impedimetric Biosensor Using the Tannin From Quercusmacrolepis as Biorecognition Element for Heavy Metals Detection. *IEEE Trans. Nanobiosci* **2015**, *14*, 694−699.
(7) Takai, E.; Hirano, A.; Shiraki, K. Effects of Alkyl Chain Length of Gallate on Self-Association and Membrane Binding. *J. Biochem.* **2011**, *150*, 165−171.
(8) Chen, Y.; Meng, J.; Zhu, Z.; Zhang, F.; Wang, L.; Gu, Z.; Wang, S. Bio-Inspired Underwater Super Oil-Repellent Coatings for Anti-Oil Pollution. *Langmuir* **2018**, *34*, 6063−6069.
(9) Baxter, N. J.; Lilley, T. H.; Haslam, E.; Williamson, M. P. Multiple Interactions between Polyphenols and a Salivary Proline-Rich Protein Repeat Result in Complexation and Precipitation. *Biochemistry* **1997**, *36*, 5566−5577.
(10) Folkers, J. P.; Laibinis, P. E.; Whitesides, G. M. Self-Assembled Monolayers of Alkanethiols on Gold: Comparisons of Monolayers Containing Mixtures of Short- and Long-Chain Constituents with Methyl and Hydroxymethyl Terminal Groups. *Langmuir* **1992**, *8*, 1330−1341.
(11) Bain, C. D.; Troughton, E. B.; Tao, Y. T.; Evall, J.; Whitesides, G. M.; Nuzzo, R. G. Formation of Monolayer Films by the Spontaneous Assembly of Organic Thiols from Solution onto Gold. *J. Am. Chem. Soc.* **1989**, *111*, 321−335.
(12) Subramanian, N.; Schmidt, R.; Wood-Adams, P. M.; DeWolf, C. E. Space-Filling Trialkoxysilane: Synthesis and Self-Assembly into Low-Density Monolayers. *Langmuir* **2010**, *26*, 18628−18630.
(13) Lahann, J.; Mitragotri, S.; Tran, T.-N.; Kaido, H.; Sundaram, J.; Choi, I. S.; Hoffer, S.; Somorjai, G. A.; Langer, R. A Reversibly Switching Surface. *Science* **2003**, *299*, 371−374.
(14) Duschl, C.; Liley, M.; Corradin, G.; Vogel, H. Biologically Addressable Monolayer Structures Formed by Templates of Sulfur-Bearing Molecules. *Biophys. J.* **1994**, *67*, 1229−1237.
(15) Moehwald, H.; Brezesinski, G. From Langmuir Monolayers to Multilayer Films. *Langmuir* **2016**, *32*, 10445−10458.
(16) Vollhardt, D.; Fainerman, V. B. Progress in Characterization of Langmuir Monolayers by Consideration of Compressibility. *Adv. Colloid Interface Sci.* **2006**, *127*, 83−97.
(17) Datta, A.; Kmetko, J.; Richter, A. G.; Yu, C.-J.; Dutta, P.; Chung, K.-S.; Bai, J.-M. Effect of Headgroup Dissociation on the Structure of Langmuir Monolayers. *Langmuir* **2000**, *16*, 1239−1242.
(18) Brezesinski, G.; Dobner, B.; Stefaniu, C.; Vollhardt, D. Monolayer Characteristics of a Long-Chain N,O-Diacyl Substituted Ethanolamine at the Air/Water Interface. *Langmuir* **2011**, *27*, 5386−5392.
(19) Boehm, C.; Leveiller, F.; Jacquemain, D.; Moehwald, H.; Kjaer, K.; Als-Nielsen, J.; Weissbuch, I.; Leiserowitz, L. Packing Characteristics of Crystalline Monolayers of Fatty Acid Salts, at the Air-Solution Interface, Studied by Grazing Incidence X-Ray Diffraction. *Langmuir* **1994**, *10*, 830−836.
(20) Miclette Lamarche, R.; DeWolf, C. Strong Headgroup Interactions Drive Highly Directional Growth and Unusual Phase Co-Existence in Self-Assembled Phenolic Films. *ACS Appl. Mater. Interfaces* **2019**, *11*, 45354−45363.
(21) Matharu, Z.; Bandodkar, A. J.; Gupta, V.; Malhotra, B. D. Fundamentals and Application of Ordered Molecular Assemblies to Affinity Biosensing. *Chem. Soc. Rev.* **2012**, *41*, 1363−1402.
(22) Tang, N. Y.-W.; Badia, A. Self-Patterned Mixed Phospholipid Monolayers for the Spatially Selective Deposition of Metals. *Langmuir* **2010**, *26*, 17058−17067.
(23) Ihalainen, P.; Peltonen, J. Covalent Immobilization of Antibody Fragments onto Langmuir−Schaefer Binary Monolayers Chemisorbed on Gold. *Langmuir* **2002**, *18*, 4953−4962.
(24) Xue, Y.; Li, X.; Li, H.; Zhang, W. Quantifying Thiol−gold Interactions towards the Efficient Strength Control. *Nat. Commun.* **2014**, *5*, 4348.
(25) Yuan, M.; Zhan, S.; Zhou, X.; Liu, Y.; Feng, L.; Lin, Y.; Zhang, Z.; Hu, J. A Method for Removing Self-Assembled Monolayers on Gold. *Langmuir* **2008**, *24*, 8707−8710.
(26) Kaganer, V. M.; Möhwald, H.; Dutta, P. Structure and Phase Transitions in Langmuir Monolayers. *Rev. Mod. Phys.* **1999**, *71*, 779−819.
(27) Jacquemain, D.; Leveiller, F.; Weinbach, S. P.; Lahav, M.; Leiserowitz, L.; Kjaer, K.; Als-Nielsen, J. Crystal Structure of Self-Aggregates of Insoluble Aliphatic Amphiphilic Molecules at the Air-Water Interface. An x-Ray Synchrotron Study. *J. Am. Chem. Soc.* **1991**, *113*, 7684−7691.
(28) Meister, A.; Weygand, M. J.; Brezesinski, G.; Kerth, A.; Drescher, S.; Dobner, B.; Blume, A. Evidence for a Reverse U-Shaped Conformation of Single-Chain Bolaamphiphiles at the Air−Water Interface. *Langmuir* **2007**, *23*, 6063−6069.
(29) Flores, A.; Ize, P.; Ramos, S.; Castillo, R. The Dioctadecylamine Monolayer: Textures, Phase Transitions, and Dendritic Growth. *J. Chem. Phys.* **2003**, *119*, 5644−5653.
(30) Ueno, M.; Kawanabe, M.; Meguro, K. Monolayer Properties of Some α, ω-Diols. *J. Colloid Interface Sci.* **1975**, *51*, 32−35.
(31) Zhang, L.; Jiang, S.; Liu, M. Configuration and Photochemical Reaction of a Bolaamphiphilic Diacid with a Diazo Resin in Monolayers and Langmuir−Blodgett Films. *J. Colloid Interface Sci.* **2003**, *261*, 417−422.
(32) Ducharme, D.; Max, J. J.; Salesse, C.; Leblanc, R. M. Ellipsometric Study of the Physical States of Phosphatidylcholines at the Air-Water Interface. *J. Phys. Chem.* **1990**, *94*, 1925−1932.
(33) Riddick, J. A.; Bunger, W. B.; Sakano, T. K. *Organic Solvents: Physical Properties and Methods of Purification*; 4th ed.; John Wiley and Sons: New York, 1986.

https://dx.doi.org/10.1021/acs.langmuir.9b03670
Langmuir 2020, 36, 2847−2857

(34) Banerjee, R.; Sanyal, M. K.; Bera, M. K.; Gibaud, A.; Lin, B.; Meron, M. Reversible Monolayer-to-Crystalline Phase Transition in Amphiphilic Silsesquioxane at the Air-Water Interface. *Sci. Rep.* **2015**, *5*, 8497.
(35) Behyan, S.; Gritzalis, D.; Schmidt, R.; Kebede, E.; Cuccia, L. A.; DeWolf, C. Structural Organization and Phase Behaviour of Meta-Substituted Dioctadecylaminobenzoquinones at the Air/Water Interface. *Phys. Chem. Chem. Phys.* **2019**, *21*, 2345−2350.
(36) Allara, D. L.; Atre, S. V.; Elliger, C. A.; Snyder, R. G. The Formation of a Crystalline Monolayer of Folded Molecules by Solution Self-Assembly of α,ω-Alkanedioic Acids on Silver. *J. Am. Chem. Soc.* **1991**, *113*, 1852−1854.
(37) Jacquemet, A.; Terme, N.; Benvegnu, T.; Vié, V.; Lemiègre, L. Collapsed Bipolar Glycolipids at the Air/Water Interface: Effect of the Stereochemistry on the Stretched/Bent Conformations. *J. Colloid Interface Sci.* **2013**, *412*, 72−81.
(38) Chen, P.; Gao, P.; Liu, M. Parallel Aligned Nanostripe Arrays in the Spreading Film of a Bolaamphiphile at the Air/Water Interface. *Colloids Surf., A* **2006**, *284-285*, 140−146.
(39) Weissbuch, I.; Guo, S.; Edgar, R.; Cohen, S.; Howes, P.; Kjaer, K.; Als-Nielsen, J.; Lahav, M.; Leiserowitz, L. Oriented Crystalline Thin Films of Tetracosanedioic Acid and Its Metal Salts at the Air−Aqueous Solution Interface. *Adv. Mater.* **1998**, *10*, 117−121.
(40) Chi, L. F.; Jacobi, S.; Anczykowski, B.; Overs, M.; Schäfer, H.-J.; Fuchs, H. Supermolecular Periodic Structures in Monolayers. *Adv. Mater.* **2000**, *12*, 25−30.
(41) Liu, X.; Wang, T.; Liu, M. Interfacial Assembly of a Series of Cinnamoyl-Containing Bolaamphiphiles: Spacer-Controlled Packing, Photochemistry, and Odd−Even Effect. *Langmuir* **2012**, *28*, 3474−3482.

https://dx.doi.org/10.1021/acs.langmuir.9b03670
Langmuir 2020, 36, 2847−2857